Beam-Waveguide Antenna Servo Design Issues for Tracking Low-Earth-Orbiting Satellites

W. Gawronski and J .A. Mellstrom
Jet Propulsion laboratory, California Institute of '1'ethnology
Pasadena, CA 91109

Abstract - The upcoming NASA missions will require tracking of low-orbit satellites. As a consequence, NASA antennas will be required to track satellites at higher rates than for the current deep space missions. This paper investigates servo design issues for the 34-m beam-waveguide (BWG) antennas that track low-orbit satellites. This includes the upgrade of the servo with the feedforward loop, monopulse controller design, and tracking error reduction through proper choice of elevation pinion location, through application of a notch filter, and through the elevation drive amplifier gain adjustment. Finally, improvement of the signal-to-noise rat io through averaging of the oversampled monopulse signal is prcscntcd.

Introduction

The National Aeronautics and Space Administration (NASA) antenna network, called the Deep Space Network (DSN), is operated by the Jet Propulsion Laboratory. It consists of several antenna types located at three sites: Goldstone (California), Canberra (Australia), and Madrid (Spain), and serves as a communication tool for space exploration. Future NASA missions will include low-orbiting satellites, which tracking require significantly higher antenna tracking rates, when compared to the deep space missions, Thus the servos for the new generation 34-m beam-waveguide (BWG) antennas should be upgraded to be able to follow commands at higher rates. The upgrades arc illustrated with the 11 S-13 BWG antenna controller design.

The existing proportional and integral (P]) controllers of the antennas satisfy the requirements for deep-space X-band (8.4 GHz) tracking. For high-rate command following a simple and reliable choice is a feedforward controller anal yzed in the paper. For tracking, a monopul se cent roller is a fast rate alternative to the existing conscan technique, The design and performance of a monopulse controller is discussed. It is shown that its performance can be improved through proper choice of the location of the elevation pinion, through the implementation of a notch filter, or through the amplifier gain adjustment. Finally, the improvement of the signal-to-noise ratio (SNR) of the monopulse signal is presented. By averaging the redundant monopulse samples the SNR improvement ranges from 7 up to 17 dB.

Feedforward Controller Design

Tracking accuracy of fast moving objects can be improved if a PI servo is augmented with a feedforward loop[1], as shown in Fig. 1. In this block diagram, G_p, G_c, G_f, and G_w denote transfer functions of the antenna's rate loop, PI controller, feed-forward gain, and wind disturbance, respectively, r is a command, y is output (elevation and azimuth angles), e is tracking error in azimuth and elevation, u is plant input, and w is wind disturbance.

In order to analyze the impact of the feed-forward gain on the closed-loop system performance, the transfer function from the command r and wind disturbance w to the tracking error e was derived. From Fig. 1, one obtains:

$$e = r - y,\ y = G_p u + G_w w,\ u = G_f r + G_c e \qquad (1)$$

Assuming $I + G_p G_c$ nonsingular, and denoting $G_o = (I + G_p G_c)^{-1}$, from Eqs. (1) one obtains

$$e = G_o(I - G_p G_f) r - G_o G_w w. \qquad (2)$$

From the above equation it follows that in the absence of wind disturbances perfect tracking ($e = 0$) is obtained for the feed-forward gain G_f such that

$$G_p(\omega) G_f(\omega) = I. \qquad (3)$$

In the case of the Deep Space Network antennas, the condition (3) is satisfied in a certain frequency range only. By inspection of the magnitudes of the plant transfer function for elevation command in Fig.2a,b (transfer functions for azimuth command arc similar), one can see that for frequencies $0 \le \omega \le 2\pi$ rad/sec ($0 \le f \le 1$ Hz), the plant transfer function G_p can be approximated with an integrator $G_p \cong G_{po} = (j\omega)^{-1} I_2$, for $0 \le \omega \le 2\pi$ rad/sec. Thus, the feed-forward differentiation

$$G_f = j\omega I_2 \qquad (4)$$

will satisfy Eq.(3) in the frequency range $0 \le \omega \le 2\pi$ rad/see, In Fig.2a, the diagonal terms of the differentiation transfer function (4) are shown with dotted lines. Their inverses (dashed lines) are equal to the plant transfer function, as in Fig.2a, for frequencies up to 1 Hz. 'l'he off-diagonal terms of (4) (transfer functions from elevation command to azimuth position, and from azimuth command to elevation position) should be zero; actually, they arc small for frequencies up to 1 Hz, as in Fig.2b.

The cl osed-loop transfer function (elevation encoder to elevation command) for a system with and without the feed-forward gain is compared in Fig.3. The figure shows that for frequencies up to 1 Hz the system with the feed-forward gain has superior tracking properties when compared with the system without fed-forward gain. This is confirmed by tracking with a trajectory as that in Fig.4. The DSS-13 antenna, with proportional gain $k_p = 0.5$ and integral gain $k_i = 1.8$ in azimuth and elevation, was investigated. Pointing errors arc shown in Fig.5, and the maximal error of 1.4 mdeg in elevation and 0.2 mdeg in cross-elevation was observed, which exceeds the requirements. However, for this controller the high frequency components of the command arc strongly amplified, as can be observed from the transfer function plots in Fig. 3, where the resonance peaks of the system with feedforward gain arc much higher than the ones of the system without feed-forward gain. As a result, any sharp change in the command may cause excessive vibrations of the antenna.

Despite the increased sensitivity y to the command inputs, the disturbance rejection of the antenna with fed-forward gain remains the same as that for the antenna without feed-forward gain. This follows from Eq. (2), where the tracking error e due to wind disturbance w is independent of the feed-forward gain G_f. Thus the pointing errors due to wind gust disturbances arc comparable with the results obtained for the DS S- 13 antenna with the PI servo, see Ref. **[2].**

Monopulse Controller Design

In monopulse tracking a deviation of an antenna from a target is detected by four slightly displaced feedhorns, each of them receiving the signal from a slightly different angle. The received beams are added and subtracted to form a sum and a difference beam. The di fference beam is zero when the target is on the antenna boresight, and the nonzero di fferencc beam produces an error signal, which is used by the monopul sc control s ystcm. Detailed

description of the monopulse technique is given in Refs. [3-6].

The monopulse tracking control system is shown in Fig.6a. It consists of the plant, monopulse feedhorns, and the monopulse controllers in azimuth (H_a) and elevation (H_e). The plant in this case is the antenna with the closed encoder position-loop. The monopulse feedhorns detect the tracking errors in azimuth (e_a) and elevation (e_e). The encoder command in azimuth is denoted r_a, and in elevation r_e. The feedhorns detect the tracking errors e_a and e_e directly, and the output signals y_a and y_e, as well as the commands c_a and c_e, are not available. Note that y_a and y_e signals arc not the encoder outputs but antenna positions related to the focal location of the RF beam.

Denote the two- nput two-output plant transfer function G

$$G = \begin{bmatrix} G_{aa} & G_{ac} \\ G_{ea} & G_{ec} \end{bmatrix} \tag{5}$$

and introduce the following notations:

$$c = \begin{bmatrix} c_a \\ c_e \end{bmatrix}, \quad r = \begin{bmatrix} r_a \\ r_e \end{bmatrix}, \quad e = \begin{bmatrix} e_a \\ e_e \end{bmatrix}, \quad y = \begin{bmatrix} y_a \\ y_e \end{bmatrix}, \quad H = diag(H_a, H_e), \tag{6}$$

so that the block diagram of monopulse tracking is now presented as in Fig.6b. From this figure it follows that

$$Y = G_c c + G_r r \tag{7}$$

where $G_c = (1+GH)^{-1}G$, $G_r = (I+GH)^{-1}$ G arc of dimension 2x2

$$G_c = \begin{bmatrix} G_{caa} & G_{cac} \\ G_{cea} & G_{cec} \end{bmatrix}, \quad G_r = \begin{bmatrix} G_{raa} & G_{rac} \\ G_{rea} & G_{rec} \end{bmatrix} \tag{8}$$

'I'he components of G have the following properties

$$|G_{aa}| \cong |G_{ee}| \cong 1, \qquad \text{for } f < f_o \tag{9a}$$

$$|G_{aa}| \ll 1, \ |G_{ee}| \ll 1, \qquad \text{for } f \gg f_o \tag{9b}$$

$$|G_{ac}| \ll 1, \ |G_{ea}| \ll 1, \qquad \text{for all } f \tag{9c}$$

as illustrated in Fig. 7. The above properties yield the following monopulse loop properties

$$y \cong c \qquad \text{for} \quad \|GH\| \gg 1 \tag{10a}$$

$$y \cong r \qquad \text{for} \quad \|GH\| \ll 1 \tag{lob}$$

$$y \cong 0.5(c + r) \qquad \text{for} \quad GH \cong 1 \tag{1 Oc}$$

in the first case of large open-loop gain the closed-loop monopulse system follows the monopulse command. In the second case of small open-loop gain the closed-loop system follows the encoder command. In the last case of unit monopulse gain the system follows the average of the monopulse and the encoder command. In order to prove this, note that for $\|GH\| \gg 1$, one obtains $\|G_r\| \ll 1$ and $\|G_c\| \cong 1$, hence $y \cong c$; for $\|GH\| \ll 1$ one obtains $\|G_c\| \ll 1$ and $G_r \cong G$, thus $y \cong r$; for $GH \cong 1$ one obtains $G_r \cong 0.5G$, thus from Eq.(7) $y = 0.5GHc + 0.5Gr$, and since $G \cong 1$ (see Eq. (9)), one obtains $y = 0.5(c + r)$.

The transfer function H of the monopulse controller is determined as follows. The monopulse bandwidth f_n, is smaller than the encoder bandwidth f_o, therefore the monopulse tracker will compensate for slowly varying error signal e. If the condition (1 Oa) is satisfied for $f < f_m$, the monopulse tracking system will follow the command c. And since $G \cong 1$ for $f < f_m$, thus $\|H\| \gg 1$ is required to satisfy the condition (1 Oa). In addition, a rapid roll-off rate for $f > f_m$ would be an advantage. However, the roll-off rate is limited through the Bode conditions, as specified in Ref. [7 p.25]. Namely, the roll-off rate in the region of the gain cross-over frequency must not exceed 40

dB/decade, and for reasonable stability margin it must actually be smaller than this. Due to this restriction the following transfer function of the monopul se tracker is chosen

$$H = \frac{2\pi f_m}{s} 1_2 \qquad (11)$$

This transfer function satisfies (10a) for $f<f_{m,}$, and has a roll-off rate of 20 dB/decade for $f>f_m$ (sw Fig.7). The parameter f_m of H is determined by analyzing the root locus of the monopulse closed-loop system with respect to f_m. The plot of real parts of closed-loop poles is shown in Fig.8. It shows that for $f_m \geq 0.067$ Hz the monopulse system is unstable. In order to maintain a reasonable stability margin, $f_m = 0.04$ Hz is chosen.

The plant transfer function G is obtained for the 1>SS-13 antenna with the encoder loop closed and the feedforward loop implemented. The magnitudes of the plant transfer function are shown in Fig.9 for azimuth command (similar plot can be obtained for elevation command). From the figure one can see that conditions (9a,b) are satisfied, but condition (9c) is violated for some frequencies from the interval $f=$ [2, 10] Hz. This violation will cause some performance deterioration.

The azimuth and elevation components of the command signal r are shown in Fig.4. The command c is slightly deviated from r by δ, i.e. $c = r+\delta$, where $\|\delta\| \ll \|r\|$. The plot of δ is shown in Fig. 10. Magnitudes of transfer functions are shown in Fig. 1 la from input r to output y, and in Fig. 1 lb from input c to output y. They indicate that the system follows low-frequency command c, high frequency command r, and low- and high-frequency command u.

An implementation of the monopulse controller requires its discretization in time. The monopulse signal is supplied with the rate f_d Hz, or with the sampling time $T = 1/f_d$ sec. in the case of the DSS-13 antenna the sampling rate is 10 Hz. The main difference between the continuous-time and the discrete-time tracker lies in a delay of the tracking error. The

monopulse closed-loop systems with sampling rates 10 and 50 Hz have been simulated. The SO-HZ sampled system has been simulated for evaluation of accuracy of the slower sampled 10-Hz system. The simulations show similar results for 10- and 50-Hz sampling, and are shown in Fig. 10 for the 10-HZ sampled system, where the solid line denotes the tracking error e, and the dashed line the deviation δ. 'l'he plots show that the pointing accuracy increased more than t we-fold in both cases. A sampling rate of 10 Hz is satisfactory to maintain the accuracy of the control system, and the 0,1-second delay dots not deteriorate the system performance.

improving Tracking Performance

As mentioned before, the implementation of the feedforward loop causes a significant excitation of flexible motion of the antenna, specifically in the elevation loop. The mode of deformation for the highest peak in the elevation-to-elevation transfer function is shown in Fig. 12. It is a bending mode of the antenna structure, strongly excited not only by the elevation command, but also by the azimuth command. It impacts the stability and performance of an antenna. This mode is extremely difficult to control with elevation and/or azimuth torques. But the following measures can be taken to reduce the impact of this mode on tracking performance: proper location of the elevation pinion, application of a notch filter, and adjustment of the amplifier gain in elevation drive.

Choosing the Elevation Pinion local ion

The antenna tracking error for the three positions of the elevation pinion: $\alpha = 0^{\circ}, 60^{\circ}$, and 90°, as in Fig. 13, have been compared in Table 1. It shows that the higher the pinion, the smaller the error. The decrease is almost proportional to $\cos a$ and can bc explained by the fact that the elevation-to-elevat ion mode is exci ted main] y by the horizontal component F_h of the elevation pinion force F_t, proportional to the $\cos \alpha$, cf. Fig. 13.

'l'able 1, Tracking error, mdeg

	EL	XEL	TOTAL
Pinion at 0°	1.43	0.14	1.44
Pinion at 60°	0.76	0.08	0.77
Pinion at 90°	0.35	0.07	0.36

Implementing a Notch Filter

"l'he critical elevation-to-elevation peak can be decreased by applying a notch filter. This narrow-band Jilter removes a component of the specified frequency from the signal, The notch Jilter transfer function is as follows

$$G_f(s) = \frac{s^2 + \omega_f^2}{s^2 + 2\delta\omega_f s + \omega_f^2} \tag{12}$$

where ω_f [*rad/s*] is filter frequency and δ is a damping coefficient which defines the bandwidth of the filter. The elevation input signal to the antenna excites the antenna vibration mode of frequency f_f =2.12 Hz, thus $\omega_f = 2\pi f_f = 13.32\ rad/s$ and $\delta = 0.2$ have been chosen. In implementation, the matching of the filter frequency and the antenna resonance frequency is not a difficult task, since this particular resonance peak is strong and dominant, thus easily detected.

The notch filter is implemented as in Fig.14. Let (A_f, B_f, C_f, D_f), (A_r, B_r, C_r, D_r) be the Jilter and the antenna rate loop state-space representations, respectively. The state-space representation of the connection is (A_o, B_o, C_o, D_o), where

$$A_o = \begin{bmatrix} A_f & 0 \\ B_r C_f & A_r \end{bmatrix}, \quad B_o = \begin{bmatrix} B_f \\ B_r D_f \end{bmatrix}, \quad C_o = [D_r C_f \ C_r], \quad D_o = D_r D_f \tag{13}$$

'I'he closed-loop properties of the antenna with and without a notch filter are compared in Fig.15, where for the system with notch filter the peak at 2.12 Hz has disappeared. 'l-hc reduction of the peak allows one to increase significantly the gain of the monopulse loop without losing stability. This gain yields about a ten-fold reduction of elevation pointing error, as follows from comparison of Fig. 16 and Fig. 10a.

Additional simulations have been performed to test the robustness of the system to filter frequency variations up to 10% of the nominal frequency, i .e. for filter frequency $f_f = f_{fn} \pm 0.1 f_{fn}$ (and f_{fn} is a nominal frequency). They show negligible deterioration of performance.

Adjusting Amplifier Gain

The impact of the critical elevation-to-elevation peak on monopulse controller stability and performance can bc reduced by adjusting the open-loop gain. For example, the gain can bc adjusted by varying the elevation drive amplifier gain. The nominal gain k_r of the elevation drive amplifier is lowered to $k_{ro} = \beta k_r$, where $\beta = 0.33$ has been chosen through simulated tests. In doing so, the rate-loop transfer function has been lowered for high frequencies, as in Fig.17. But the feedback gain, which contains an integrator, retains the tracking properties for low frequencies of the closed-loop transfer function, while the higher frequency part of the transfer function is not compensated, lowering the critical peak cf. Fig. 18. This simple approach allows one to increase gain of the monopulse loop, producing an improvement in tracking performance similar to that with the notch filter in Fig, 16. The explanation is as follows: Let G be the transfer function of the rate loop model from elevation-to-elevation, and K the transfer function of the PI controller. The closed-loop transfer function GO is

$$G_o = \frac{KG}{1+KG} \tag{14}$$

Since K consist of an integrator, therefore $|K| \to \infty$ for $\omega \to 0$, and $|K| \to 0$ for $\omega \to \infty$. It yields $|GO| \to 1$ for $\omega \to 0$, and $|GO| \to 0$ for $\omega \to \infty$, thus tracking for low frequencies is preserved, and the peaks in higher frequencies arc suppressed. This can be seen in Fig. 18, where the low-frequency part of the closed-loop transfer function is the same, equal to 1 for $\beta = 1$ and @=0.33, but for higher frequencies the transfer function for $\beta = 0.3$ is lower than for $\beta = 1$.

improving SNR

A monopulse signal is typically contaminated with measurement noise of significant intensity. Noise intensity is measured with the signal-to-noise ratio (SNR)

$$SNR = 10 \log_{10} \frac{P_s}{P_n} \quad [\text{dB}] \tag{15}$$

where P_s, P_n are signal and noise powers, respectively. The noise impacts the pointing accuracy of the control system. Here a simple method that improves SNR is discussed.

The monopulse signal $u(i\Delta t)$ consists of a true measurement $u_o(i\Delta t)$ and a noise $n(i\Delta t)$

$$u(iAt) = u_o(i\Delta t) + n(iAt) \tag{16}$$

where $u_o(i\Delta t) = y_o(i\Delta t) - y(i\Delta t)$. It is assumed initially that the noise $n(i\Delta t)$ is a white noise with zero mean, $E(n(iAt)) = O$, where $E(.)$ is the expectation operator. The assumption is the worst-case scenario. White noise consists of components of all frequencies of equal intensity s_o, up to the Nyquist frequency f_c. Typically, the measurement noise is rather a high-frequency noise, thus its impact on system performance is less severe than the white noise.

The monopulse signal $u(i\Delta t)$, shown in Fig. 19 for sampling time **At=-** 0.02.$ is transmitted to the antenna controller in clusters every N samples (typically $N=5$), thus the new sampling period is

$$\Delta T = N \Delta t \tag{17}$$

and a cluster $U(i\Delta T)=\{u_1(i\Delta T), u_2(i\Delta T),\ldots, u_N(i\Delta T)\}$, consists of N measurements $u_k(i\Delta T)$

$$u_k(i\Delta T) = u(i\Delta T + k\Delta t), \qquad k=1,\ldots,N \tag{18}$$

The mean value, $m_k = E(u_k(i\Delta t))$, and the variance, $\sigma_k = E(\Delta u_k(i\Delta T))^2$, of each component are the same in the cluster

$$m_k = m_N, \quad \sigma_k^2 = \sigma_N^2, \quad k=1,\ldots,N \tag{19}$$

This assumption has the following meaning: The value of $u_o(i\Delta t)$ is considered constant within the period A 7' if the reaction of the antenna to $u_o(t_o + i\Delta t)$ is the same as to $u_o(t_o + N\Delta t)$ for $i = 1,\ldots,N$. 'l'his property has been confirmed by the earlier simulations reported in Ref. [8].

Although the monopulse signal is sent to the controller in clusters, only the last component, $u_N(i\Delta T)=u(i\Delta T + N\Delta t)$, is used to drive the monopulse controller. This excess information is used to reduce the signal-to-noise ratio by averaging the signal within a cluster, The average value, $u_{av}(i\Delta T)$, of the monopulse signal within the cluster of N samples is obtained

$$u_{av}(i\Delta T) = \frac{1}{N} \sum_{k=1}^{N} u_k(i\Delta T) \tag{20}$$

It is shown in the Appendix that in the case of white noise the mean value (m_{av}) of the averaged process, $u_{av}(i\Delta T)$, and the mean value (m_N) of the non-averaged process, $u_N(i\Delta T)$, are the same, while the variance of the averaged

process (σ^2_{av}) is smaller than the variance of the non-averaged process (σ^2_N) by the factor N

$$m_{av} = m_N, \qquad \sigma^2_{av} = \frac{\sigma^2_N}{N} \tag{21}$$

Define r_s, the ratio of variances of non-averaged and averaged signal

$$r_s = \frac{\sigma^2_N}{\sigma^2_{av}} \tag{22a}$$

and its logarithmic counterpart, an SNR increase, ΔSNR,

$$\text{ASNR} = SNR_{av} - SNR = 10 \log_{10} r_s \ [\text{dB}] \tag{22b}$$

then for white noise, from the definition (15), one obtains $r_s = N$ and $\Delta SNR = 10 \log_{10} N \ [dB]$.

Consider high-frequency noise with a constant spectrum within the interval $[f_o \ f_c]$, such that $0 < f_o < f_c$, f_o is a cut-off frequency (the lowest frequency component of the noise) and f_c is the Nyquist frequency, $f_c = 0.5/\Delta t$. Results of noise reduction for the high-frequency noise, obtained through simulations, are shown in Fig.20. From this ratio r_s versus cut-off frequency f_o plot it is evident that the high-frequency noise is more suppressed through averaging than the white noise (r_s increases from 5 in the case of white noise to SO in the case of high-frequency noise for cut-off frequencies of 8 Hz and higher, and SNR incrcasc, ASNR, is from 7 to 17 dB, respectivel y), These results have also been confirmed by simulations of monopulse tracking with SNR ==20 dB, where the elevation pointing error for the case of non-averaged signal is shown in Fig.21a, and the same error for the averaged signal is shown in Fig.2 lb, with the noise power ratio $r_s = 4.7$ (SNR increase ASNR = 6.7 dB), which is C1OSC to the predicted $r_s = 5$ ($\Delta SNR = 7$ dB).

Conclusions

It has been shown that the feedforward upgrade of the existing DSN antenna servos improves tracking at higher rates, and that monopulse tracking is an appropriate replacement of the conscan technique for the considered rates. A sampling rate of 10 Hz is satisfactory to maintain the accuracy of the monopulse control system, and the 0.1 -second delay does not deteriorate the system performance. Re-positioning of the elevation pinion, or implementation of a notch filter, or adjustment of amplifier gain serve as a tools for improving tracking accuracy. The monopulse SNR is improved through averaging the high-frequency sampled signal.

Appendix, Proof of Eq.(21).

The first part of Ilq.(21) follows from the definition of the averaged process (20) and the equality of mean values in the cluster, Eq.(19). Namely

$$m_{av} = \frac{1}{N} \sum_{k=1}^{N} E(u_k(i\Delta T)) = \frac{1}{N} \sum_{k=1}^{N} m_k = m_N \qquad (A1)$$

In order to prove the second part of EA.(21), denote

$$\mathrm{Auk(iAT)} = u_k(i\Delta T) - u_o(N\Delta t) = n_k(i\Delta t), \qquad (A.2)$$

$$n_k(i\Delta T) = n(i\Delta T + k\Delta t), \quad k = 1,\ldots,N. \qquad (A.3)$$

and

$$\Delta u_{av}(i\Delta T) = \frac{1}{N} \sum_{k=1}^{N} \Delta u_k(i\Delta T) \qquad (A.4)$$

thus the variance of the averaged process is

$$\sigma_{av}^2 = E(\Delta u_{av}(i\Delta T))^2 = \frac{1}{N^2} \sum_{k,l=1}^{N} E(\Delta u_k(i\Delta T)\ \Delta u_l(i\Delta T)) \qquad (A.5)$$

Since the white noise is not correlated, that is

$$E(n_k(i\Delta T)n_l(i\Delta T)) = 0 \quad for \quad k \neq l \qquad (A.6)$$

therefore

$$E(\Delta u_k(i\Delta T)\ \Delta u_l(i\Delta T)) = \mathrm{O}, \qquad \text{for } k \neq l \qquad (A.7)$$

Introducing Eq.(A.7) and Eq.(19) to Eq.(A.5)

$$\sigma_{av}^2 = \frac{1}{N^2} \sum_{k=1}^{N} E(\Delta u_k(i\Delta T)^2 = \frac{1}{N^2} \sum_{k=1}^{N} \sigma_k^2 = \frac{\sigma_N^2}{N} \qquad (A.8)$$

proves the second part of Eq.(21).

Acknowledgment

This research was performed at the Jet Propulsion Laboratory, California Institute of Technology, under a contract with the National Aeronautics and Space Administration.

References

[1] W. Gawronski: "Feedforward Control Upgrade of the Deep Space Network Antennas," *TDA Progress Report,* vol .*42-110,* 1992.

[2] W. Gawronski, B. Bienkiewicz, and R. Ii. Hill: "Wind-Induced Dynamics of the Deep Space Network Antennas," *33rd AIAA Structures, Structural Dynamics, and Materials Conference,* Dallas, TX, 1992; also accepted for publication in *Journal of Sound and Vibration, 1993.*

[3] *D.* K, Barton: *Modern Radar System Analysis,* Artech House, 1988.

[4] D. R. Rhodes: *Introduction to Monopulse*, McGraw Hill, New York, 1959.

[5] J. C. Toomay: *Radar Principles for the Non-Specialist*, Van Nostrand Reinhold, New York, 1989.

[6] G. Biernson: *Optimal Radar Tracking Systems*. Wiley-l nterscience, New York, 1990.

[7] J .M. Maciejowski: *Multivariable Feedback Design*. Addi son-Wesley, Wokingham, 1 9 8 9 .

[8] W. Gawronski, and J.A. Mellstrom, "Control and Dynamics of the Deep Space Network Antennas". in: *Control and Dynamics systems, ed, C .T. Leondes*, vol.57, Academic Press, Ncw York, 1993.

Figures:

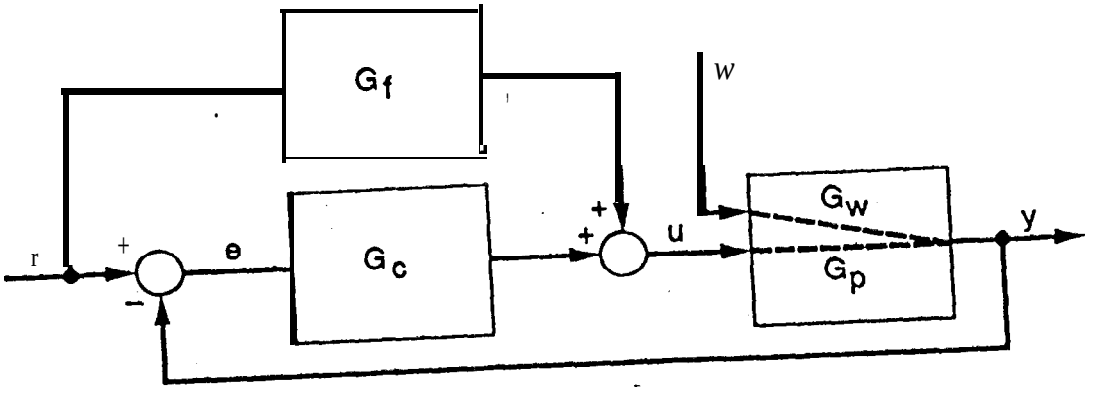

GAWRONSKI, FIG. 1

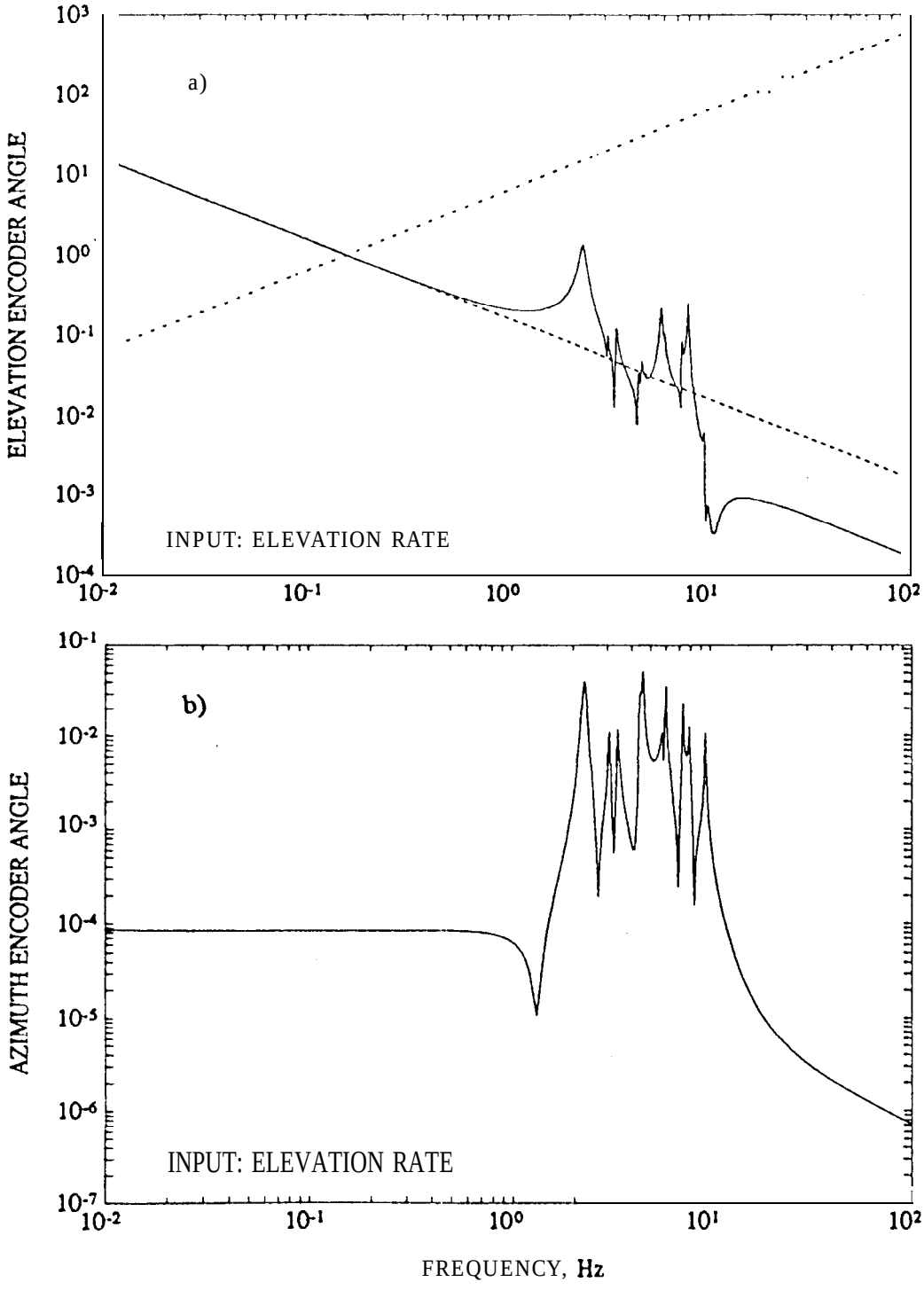

GAWRONSKI, FIG.2

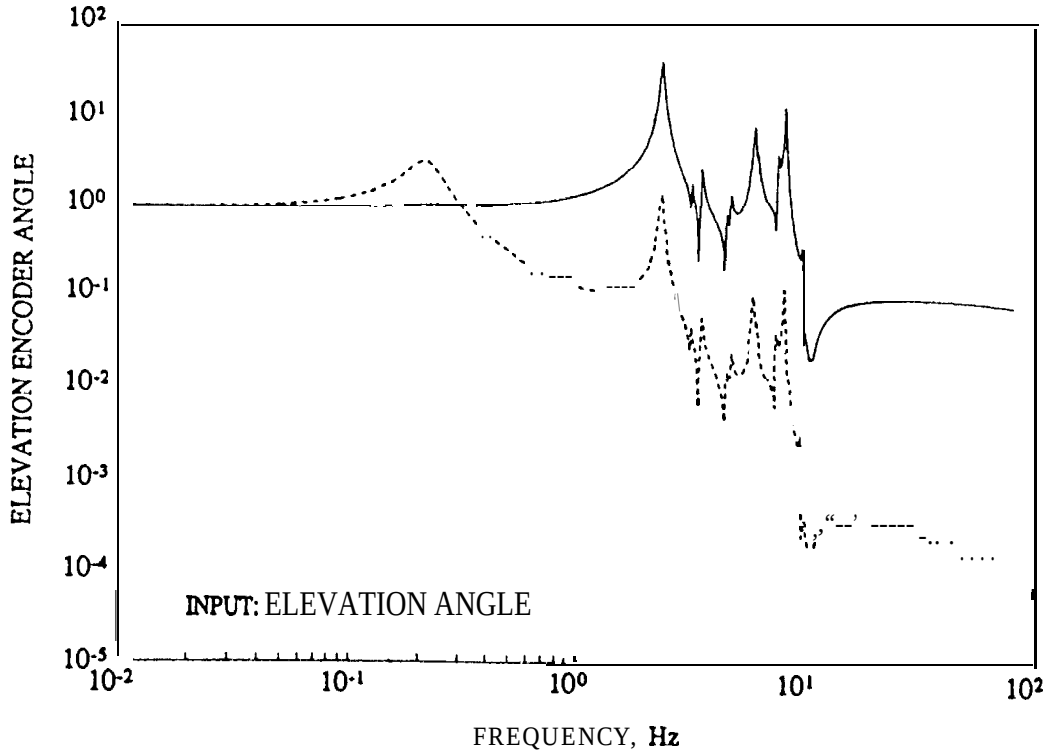

GAWRONSKI, FIG.3

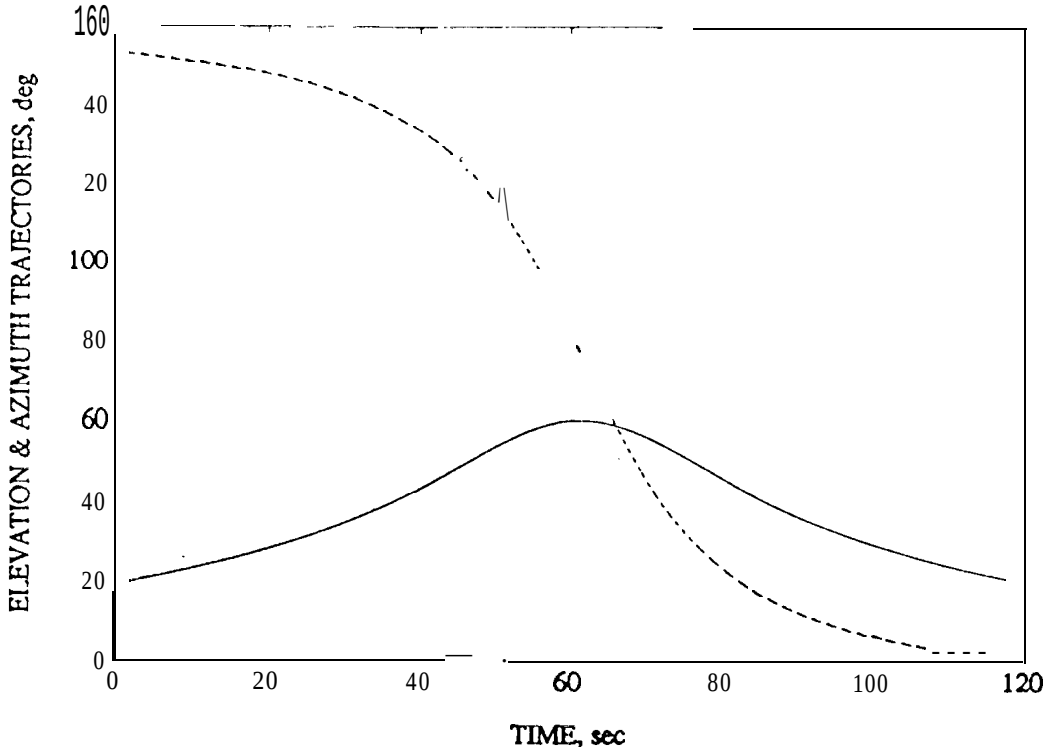

GAWRONSKI, FIG.4

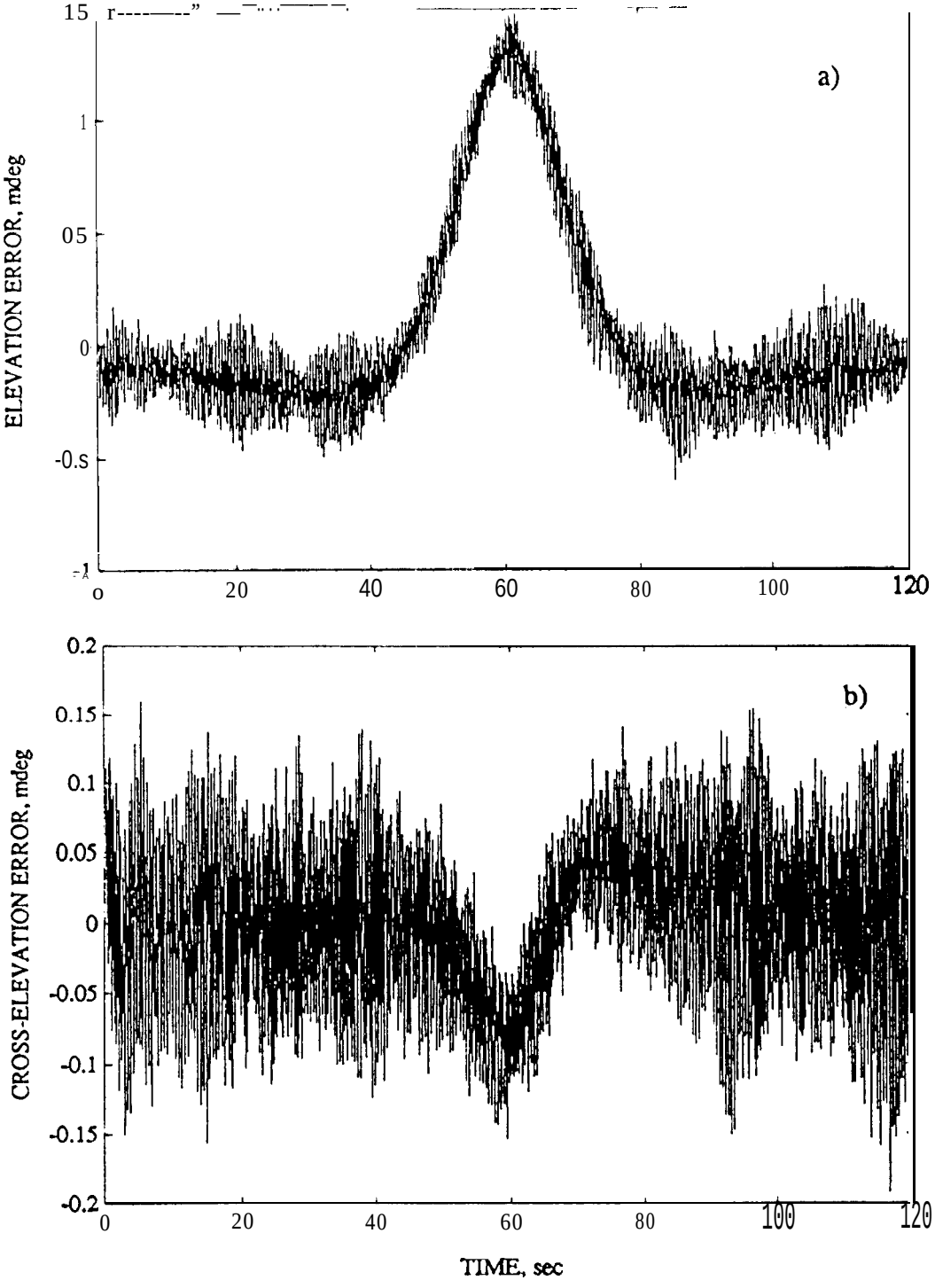

GAWRONSK1, FIG.5

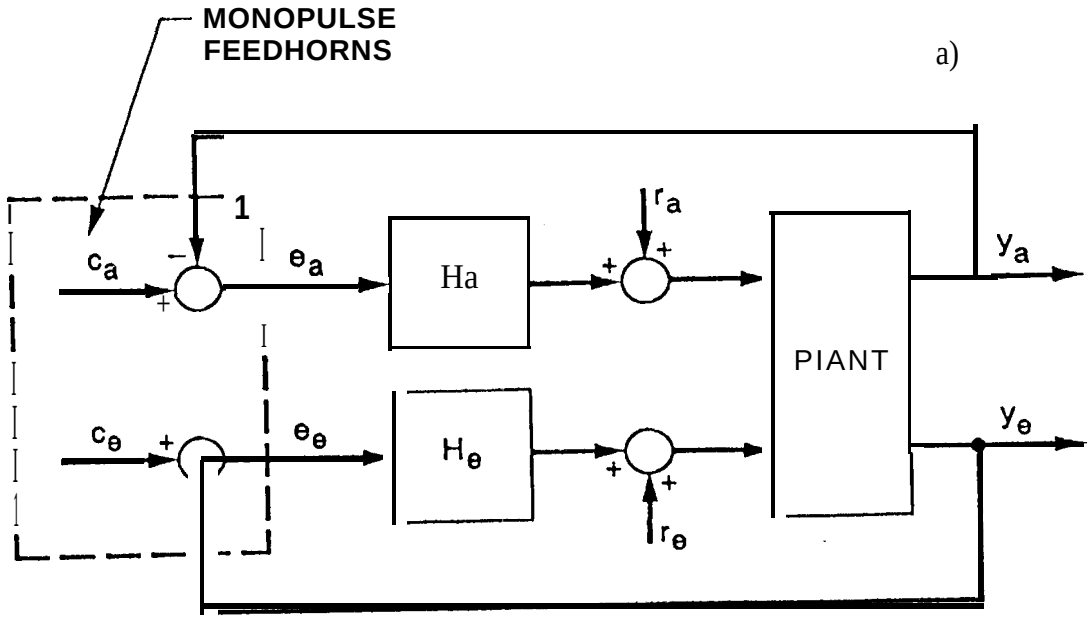

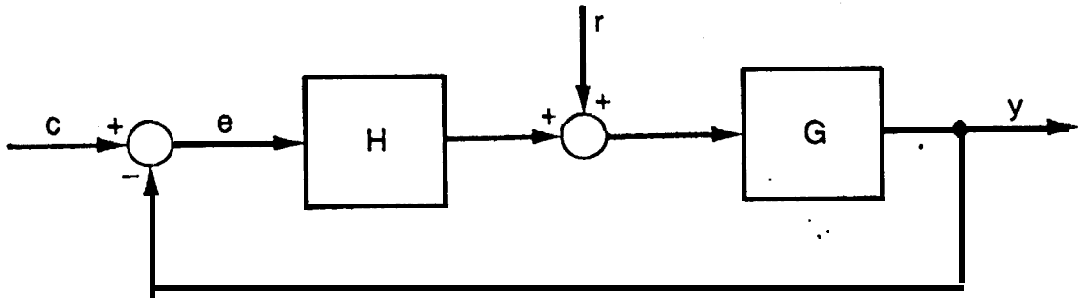

GAWRONSKI, FIG.6

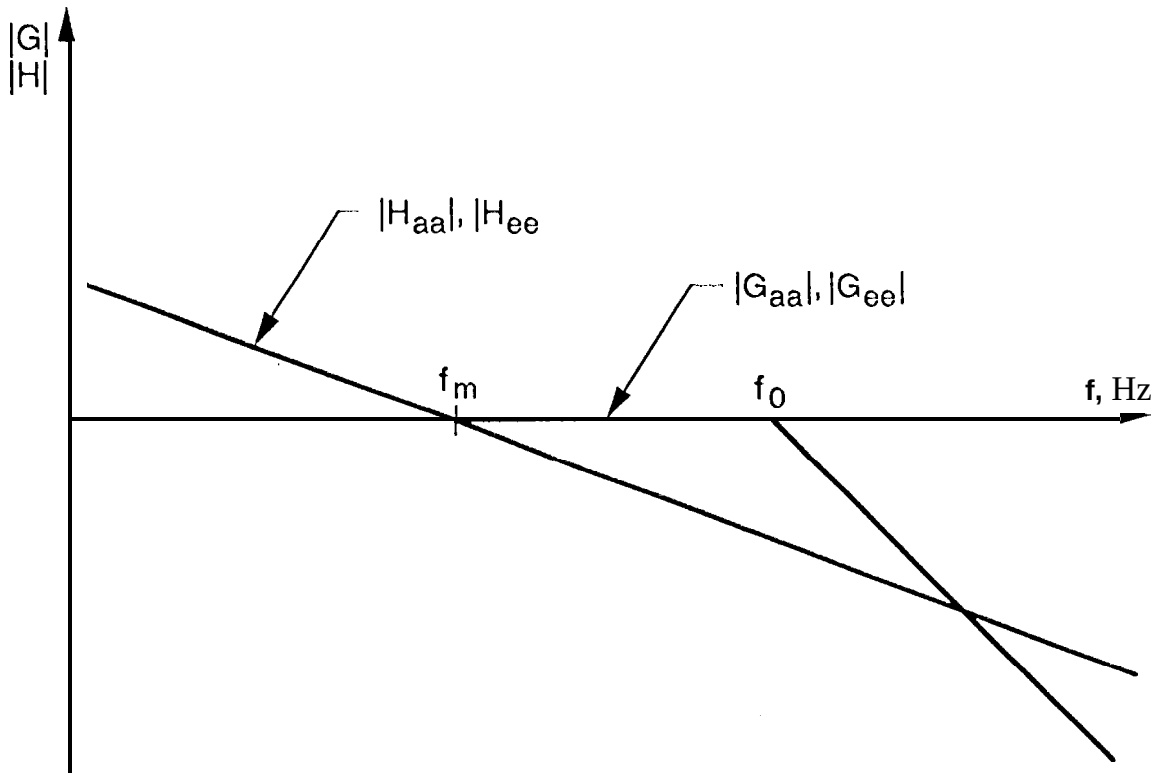

GAWRONSKI, FIG .7

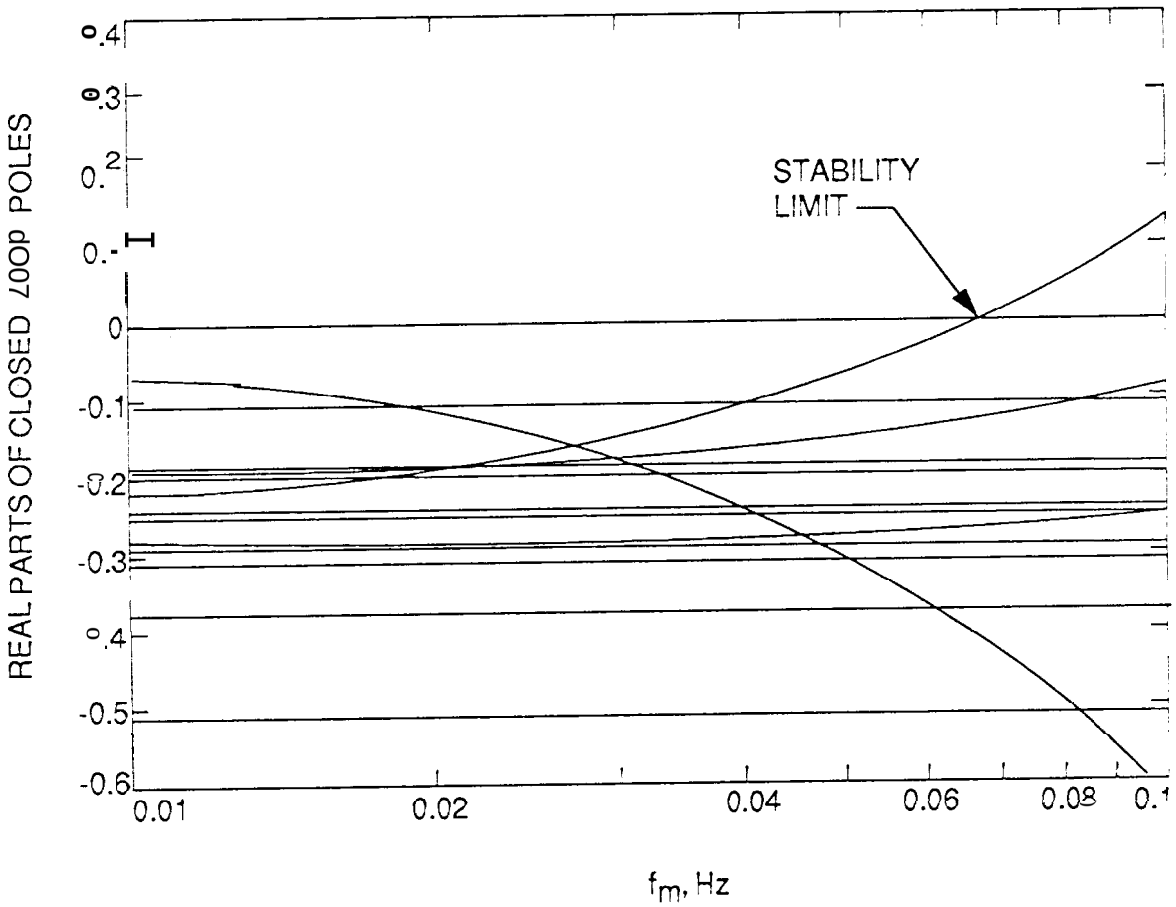

GAWRONSKI, FIG.8

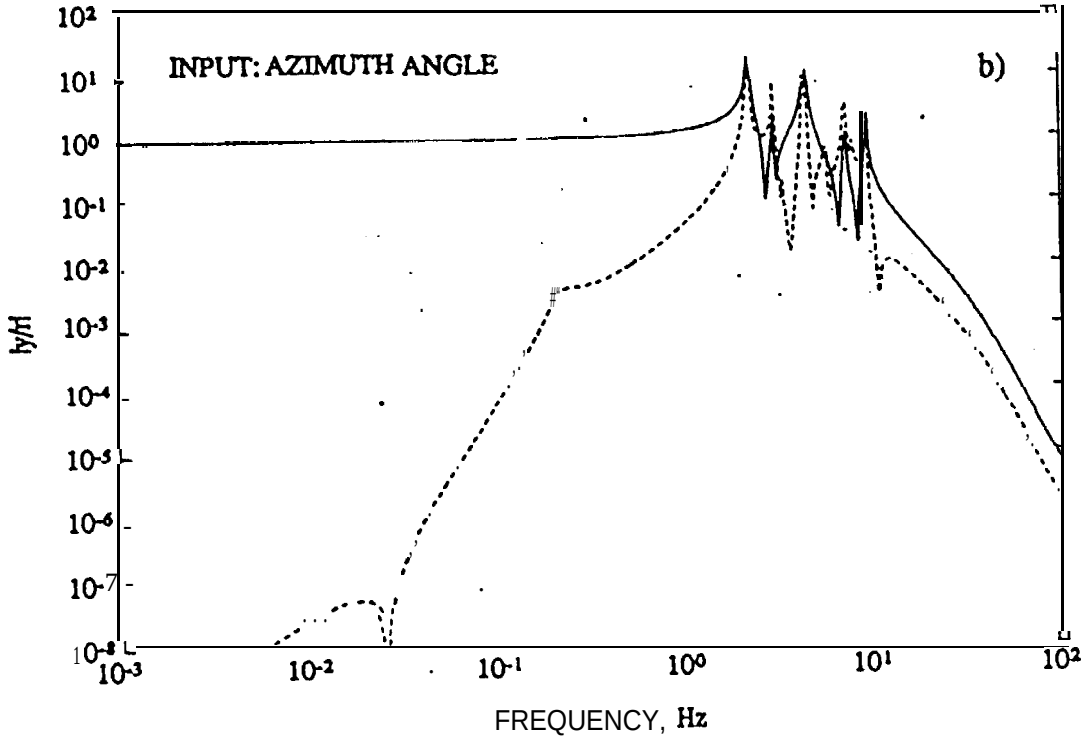

GAWRONSKI, FIG.9

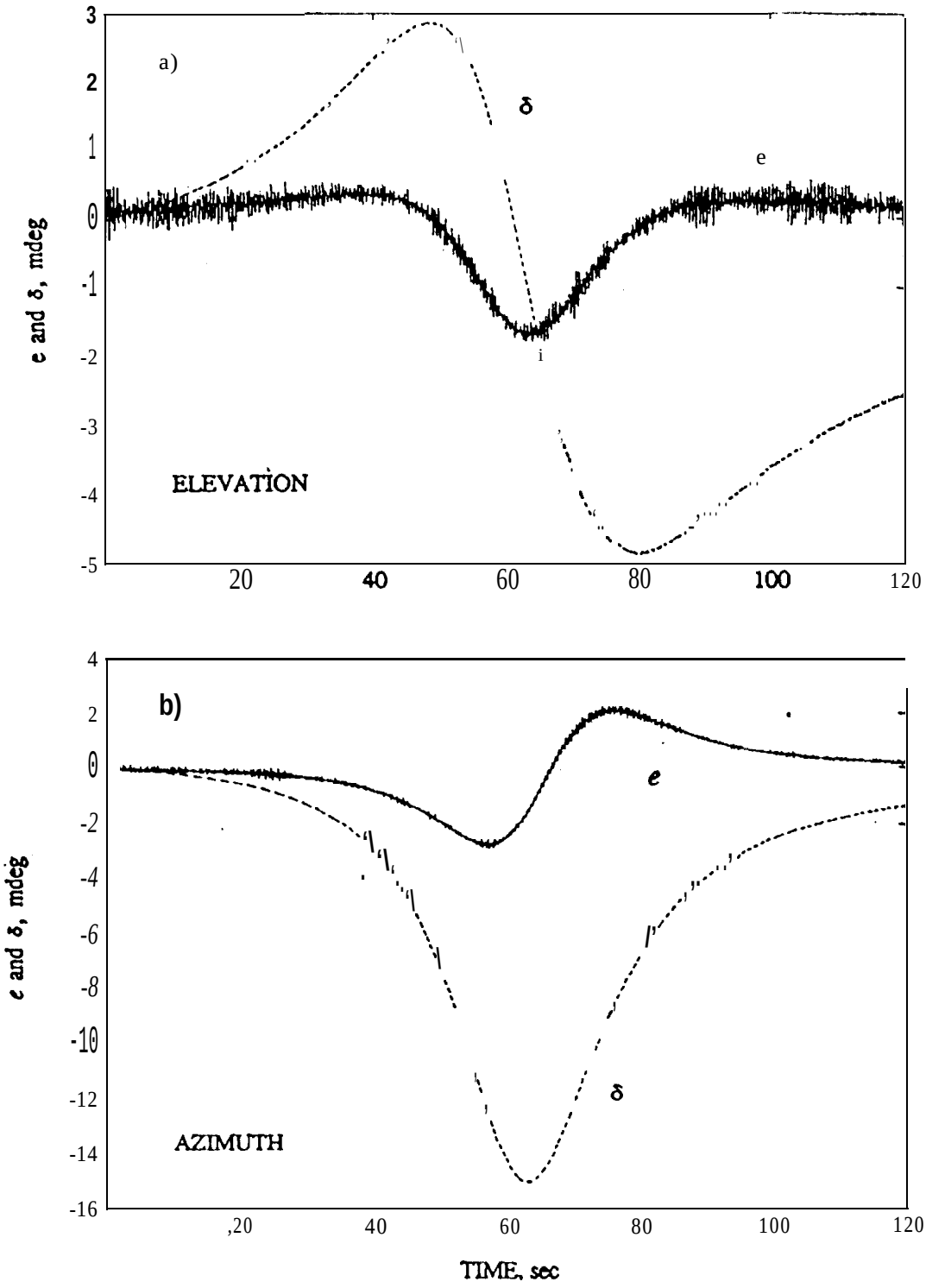

GAWRONSKI, FIG. 10

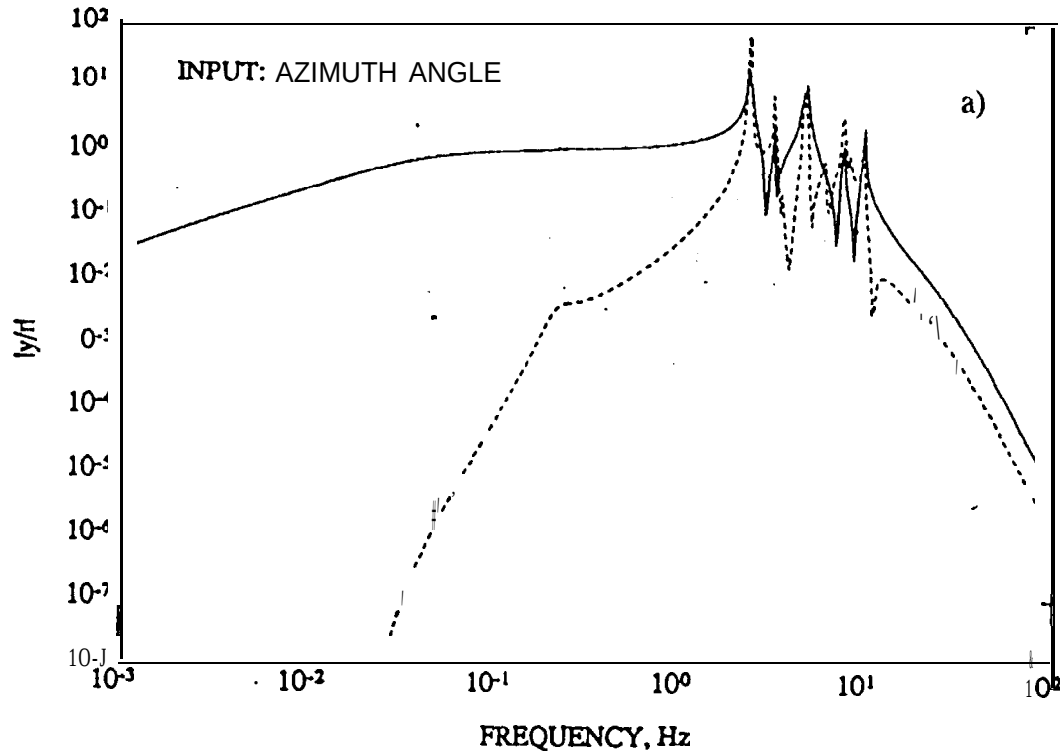

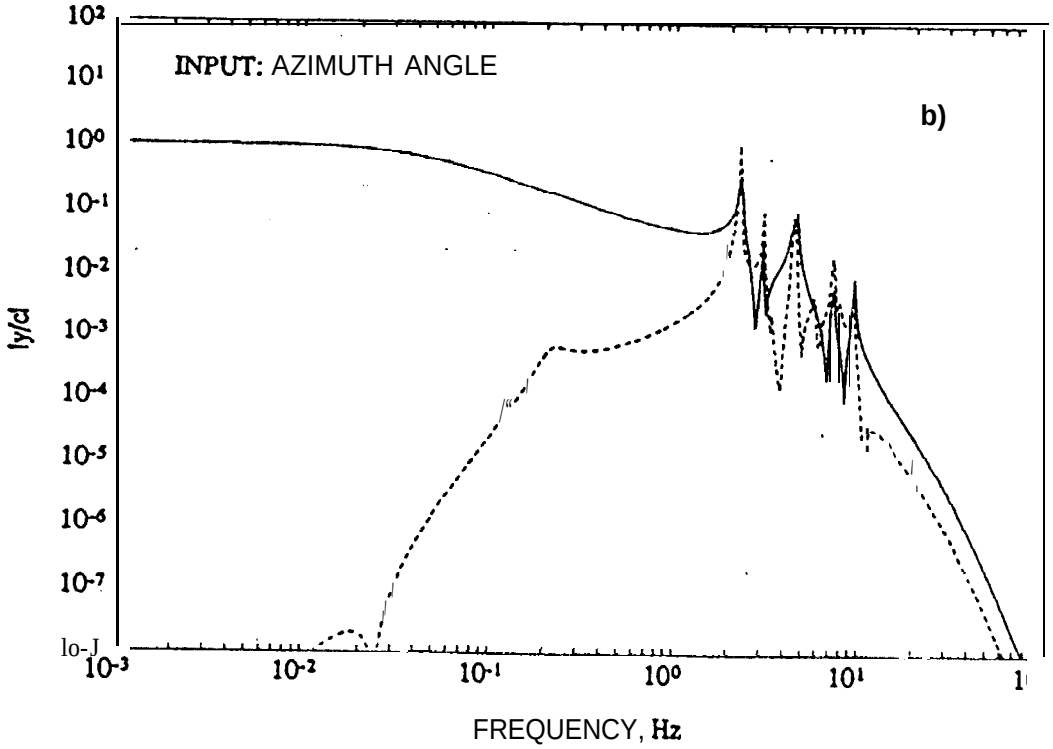

GAWRONSKI, FIG. 11

I-DEAS VI: FE_Modeling_&_Analysis

17-DEC-92 09:21:53

Units : IN

Database: new
View : No stored View
Task: Post Processing

Display : No stored Option
Model Bin: 1-MAIN

$TITLE = A07C.DAT

EE

LOAD SET: 1

DISPLACEMENT - NORMAL MIN: 0.00 MAX: 6505.63

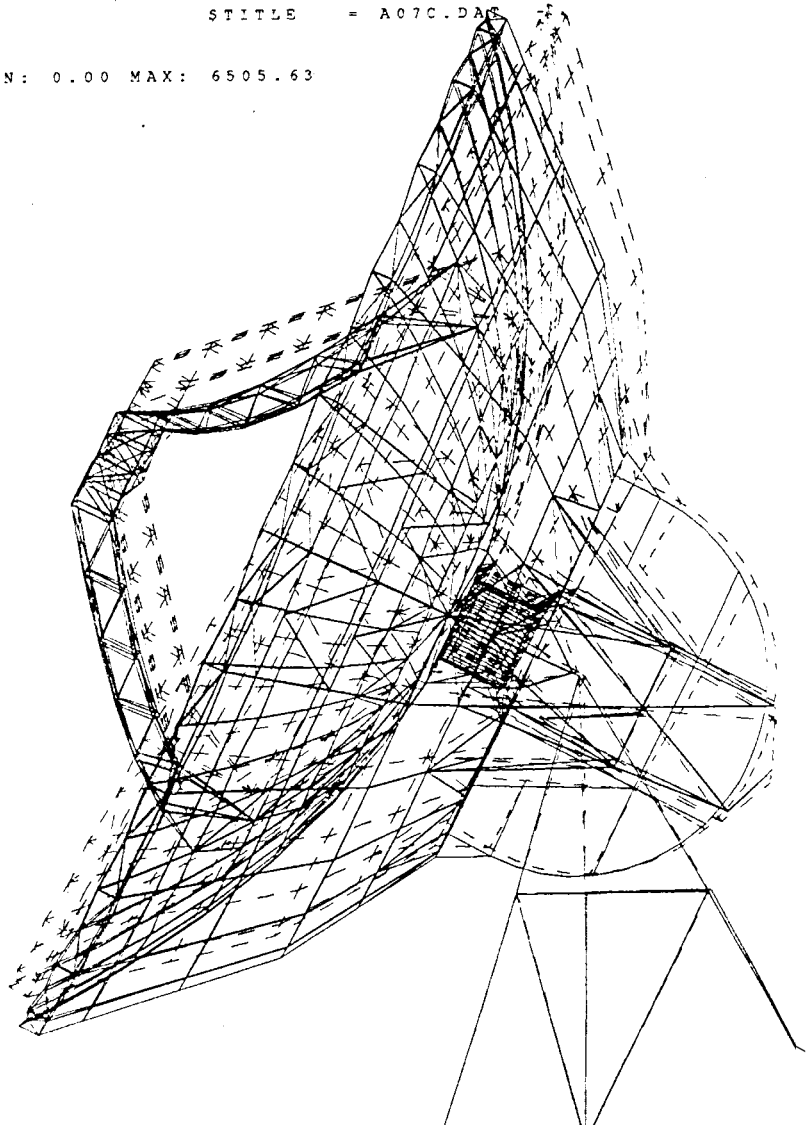

GAWRONSKI, FIG.12

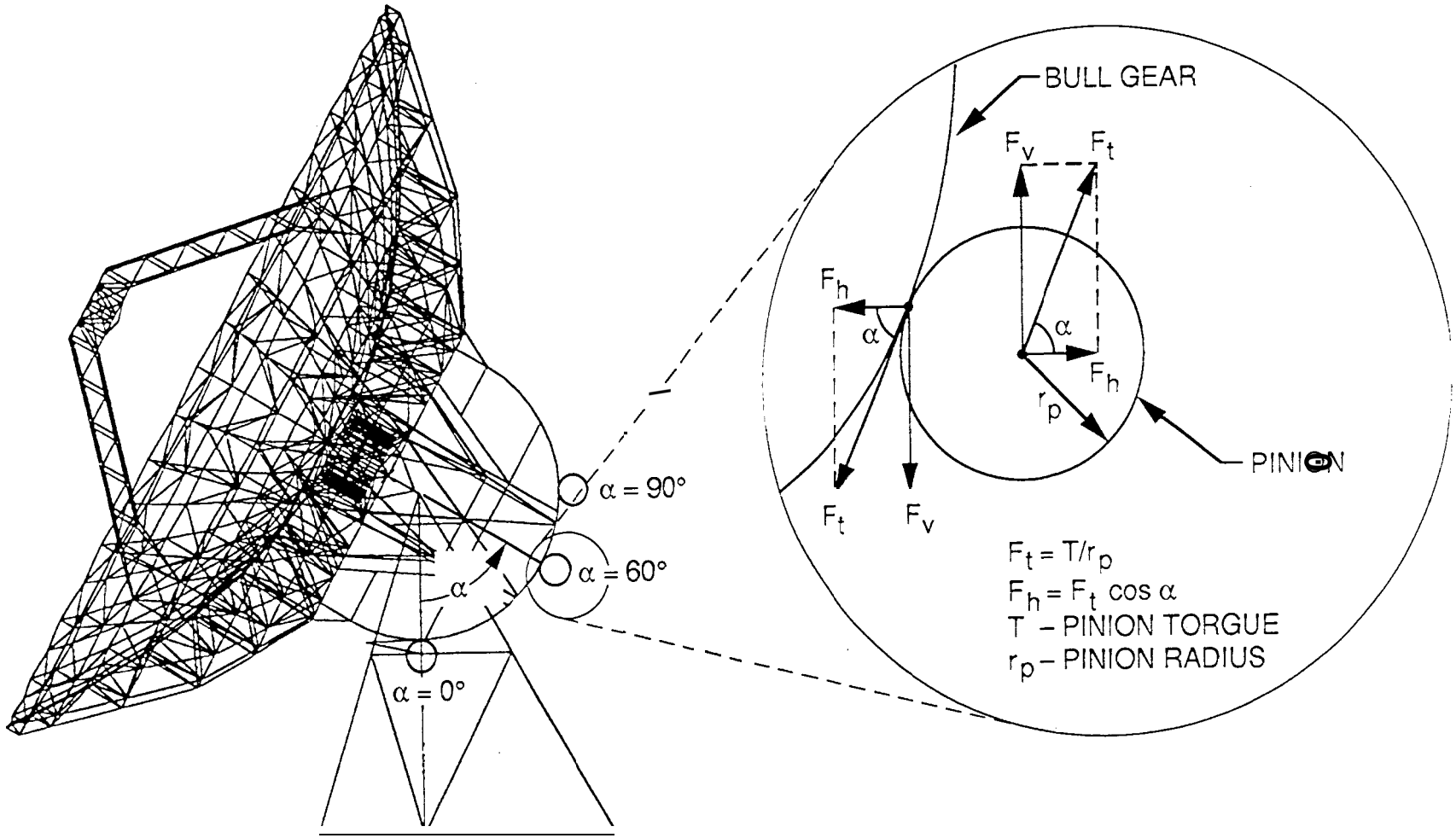
α = 90°
α = 60°
α = 0°
α
BULL GEAR
F_v
F_t
F_h
α
α
F_h
r_p
PINION
F_t
F_v
$F_t = T/r_p$
$F_h = F_t \cos \alpha$
T – PINION TORGUE
r_p – PINION RADIUS

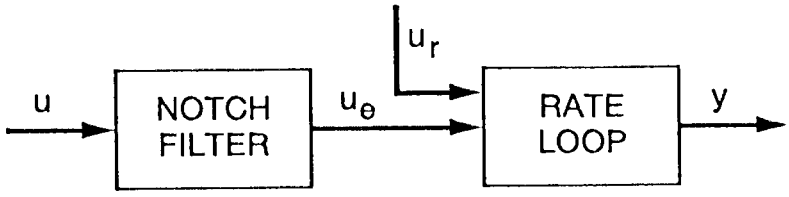

GAWRONSKI, FIG. 14

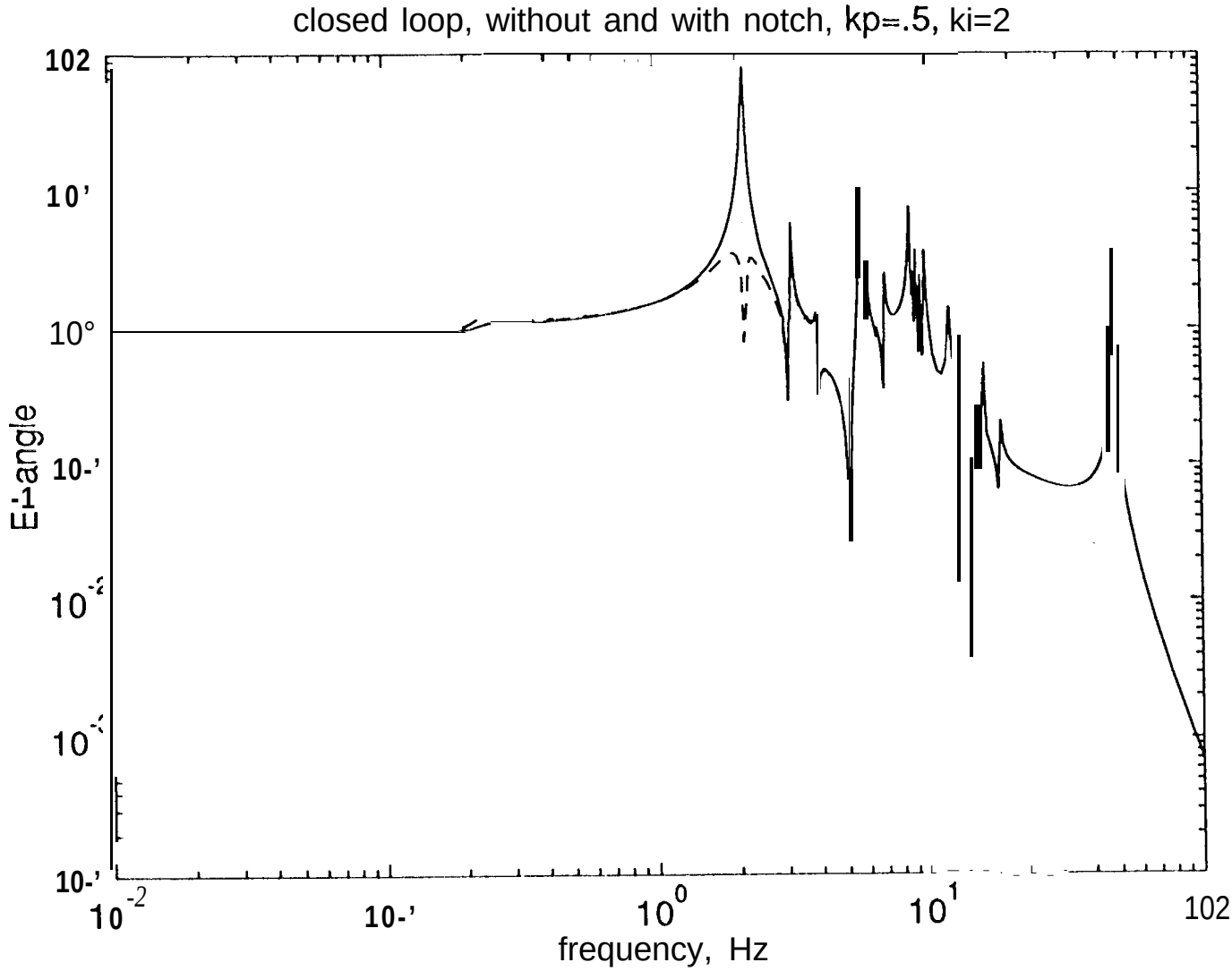

GAWRONSKI, FIG. 15

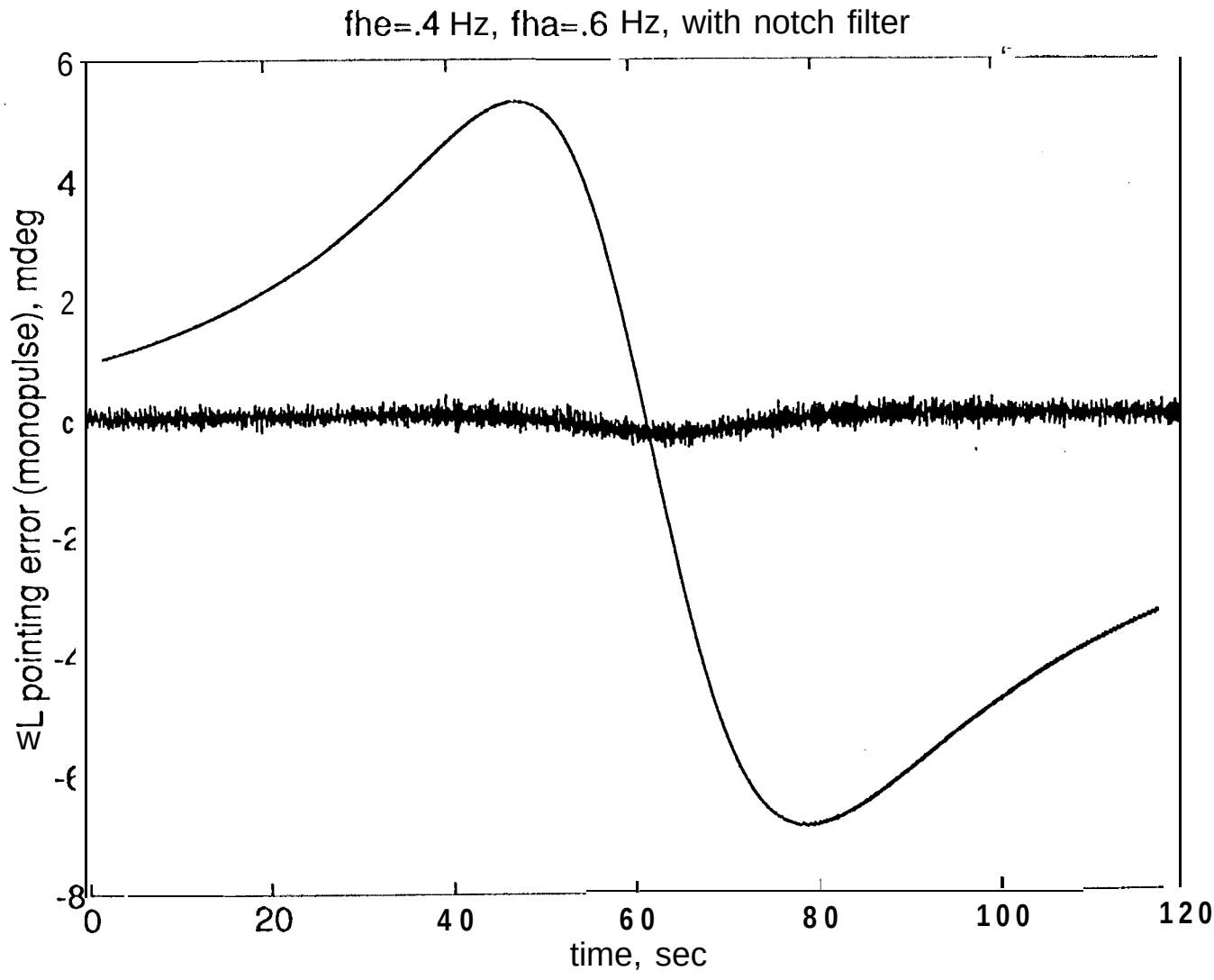

GAWRONSKI, FIG. 16

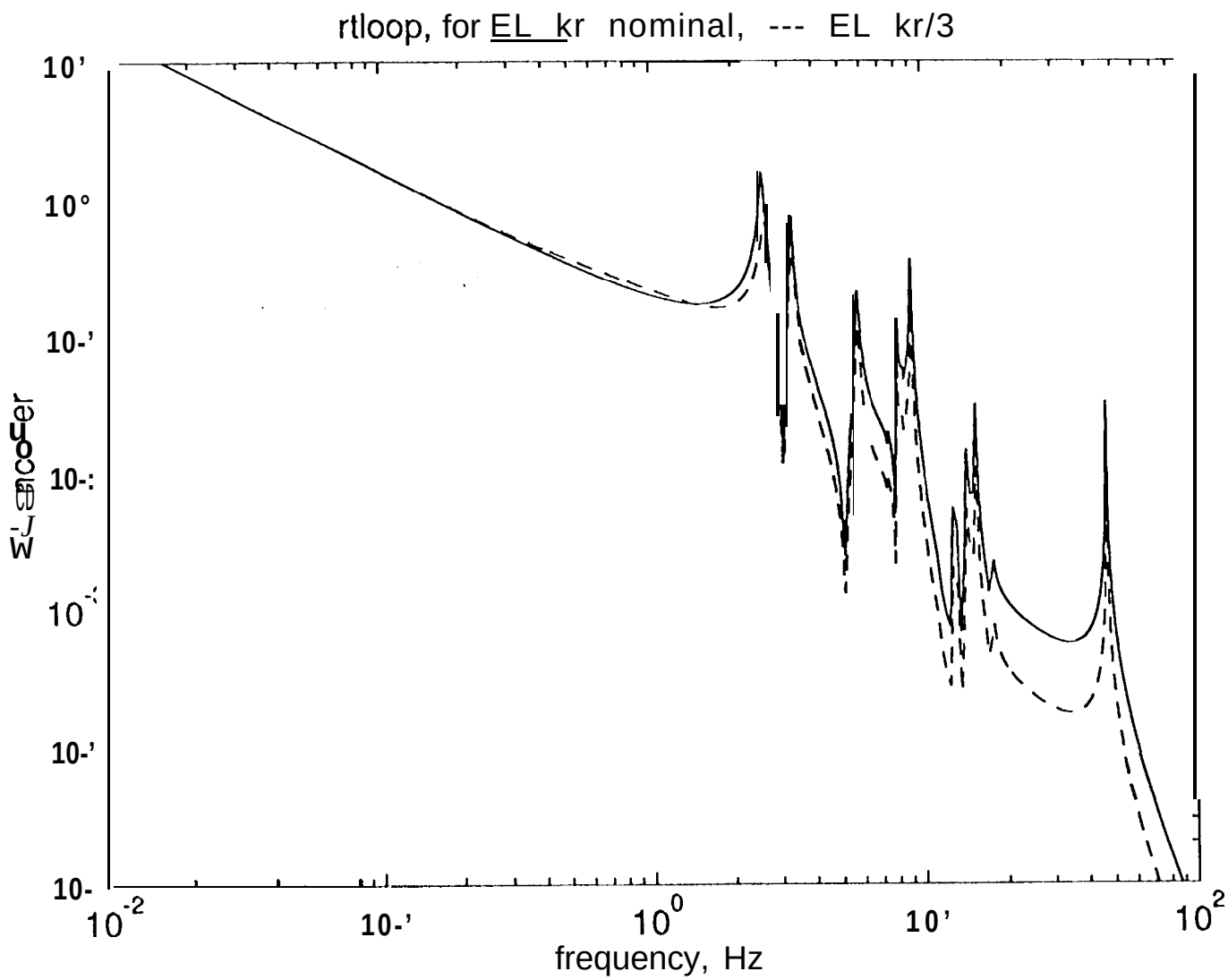

GAWRONSKI, FIG. 17

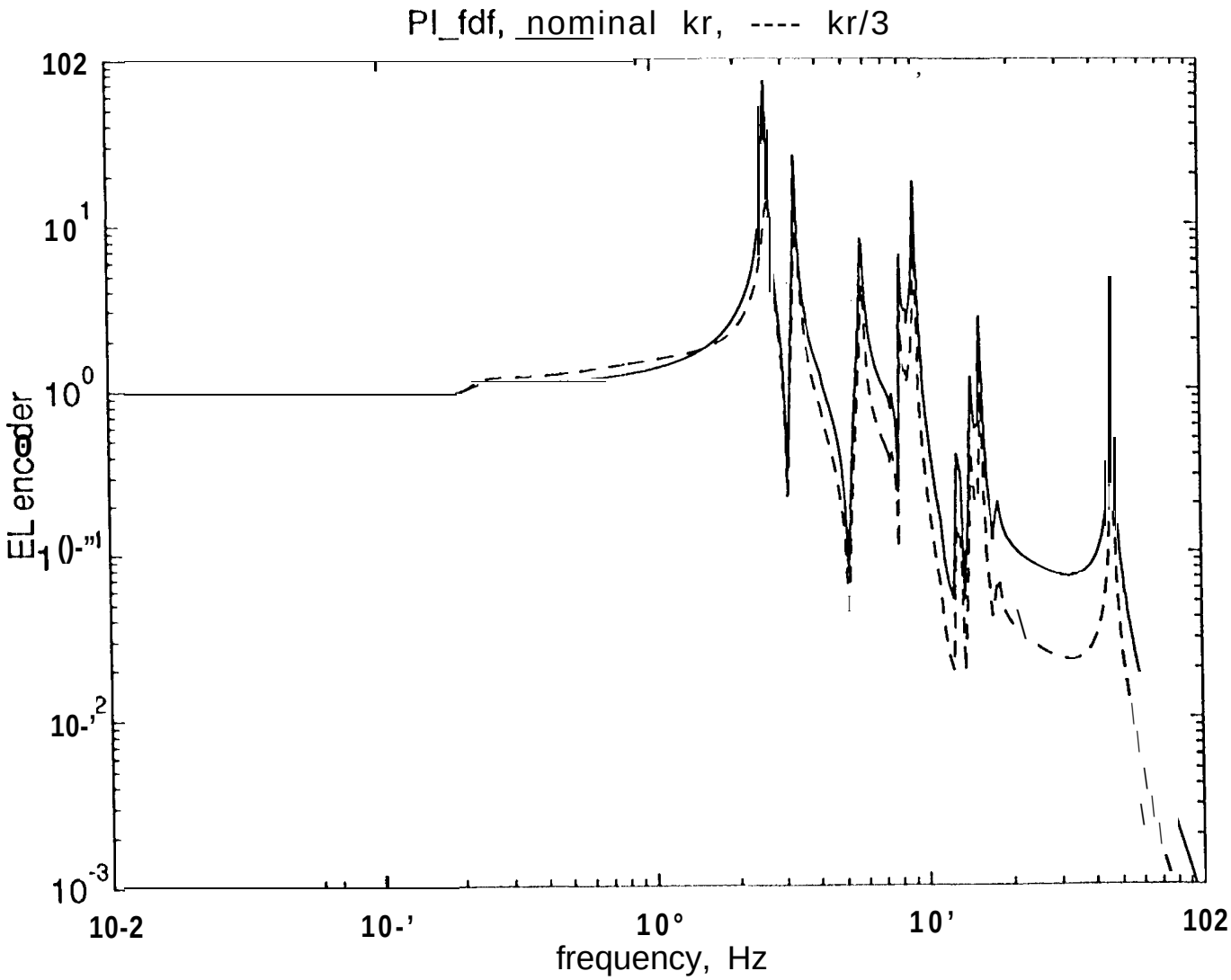

GAWRONSKI, FIG, 18

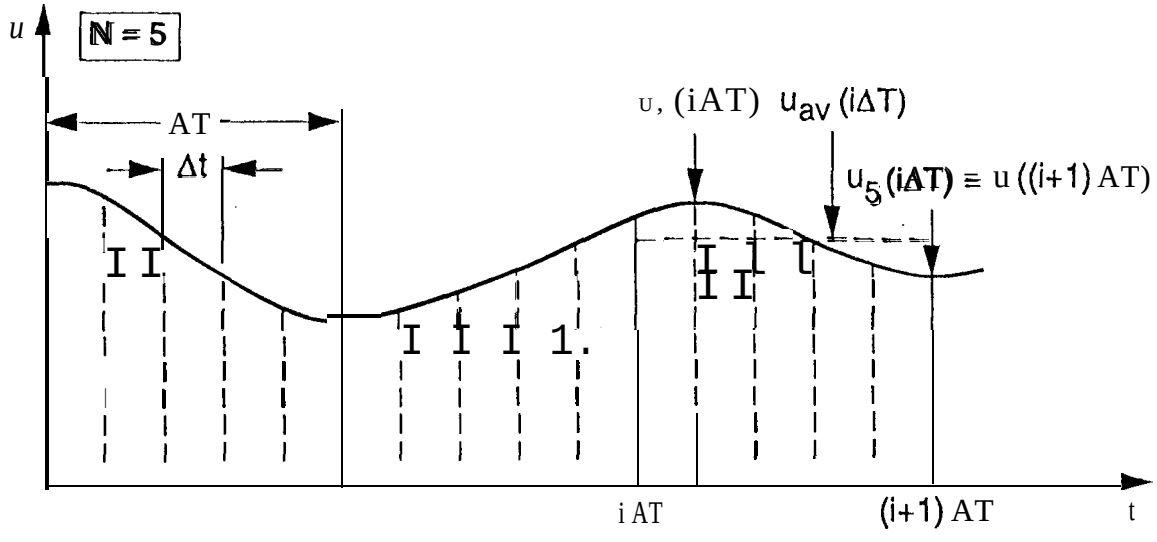

GAWRONSKI, FIG. 19

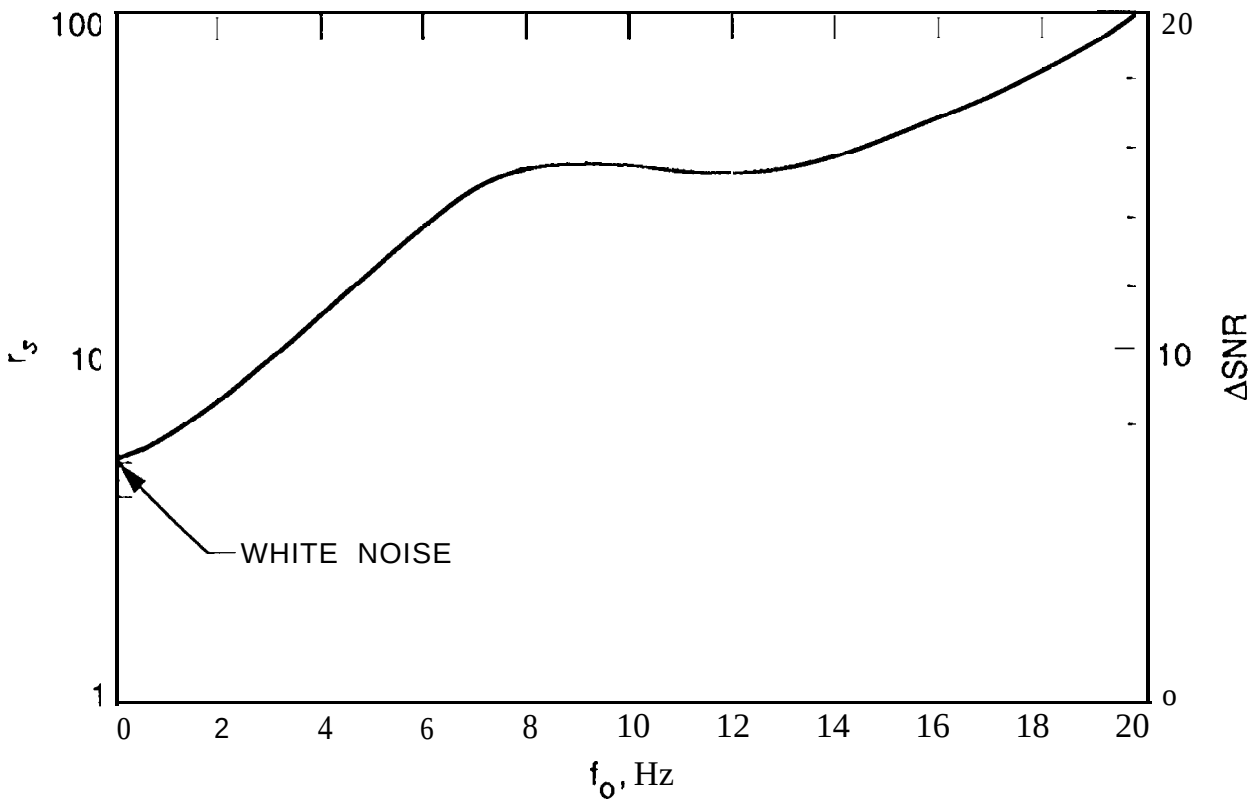

GAWRONSKI, FIG.20

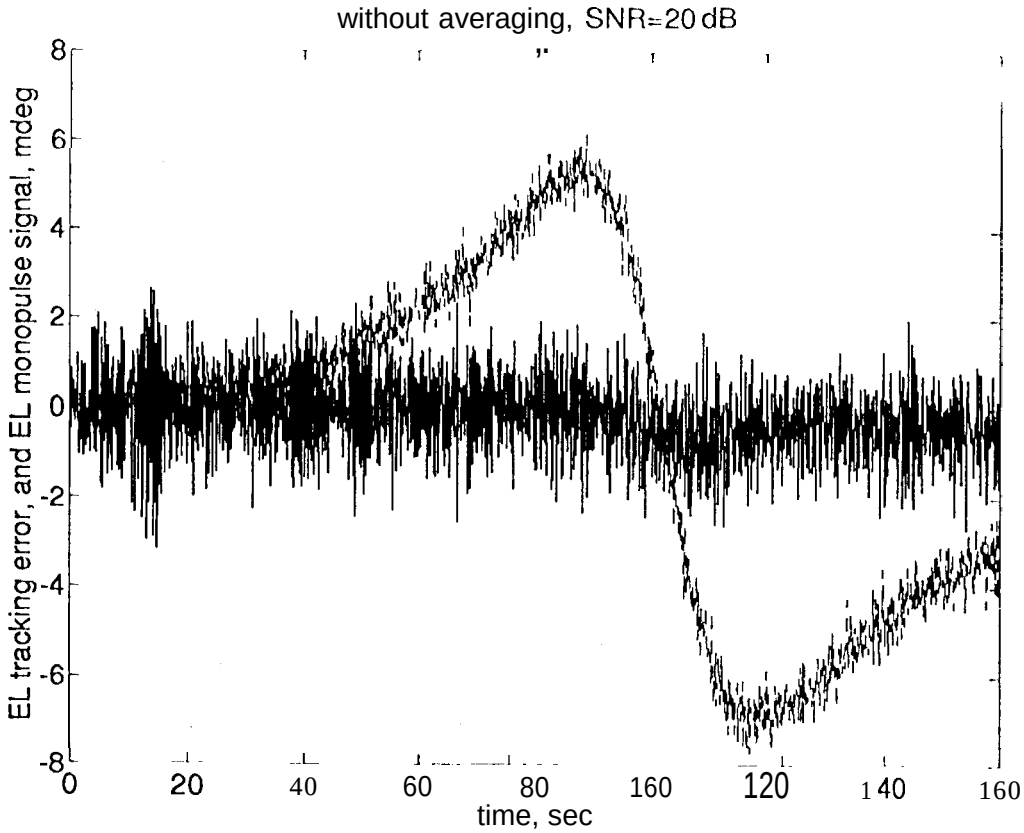

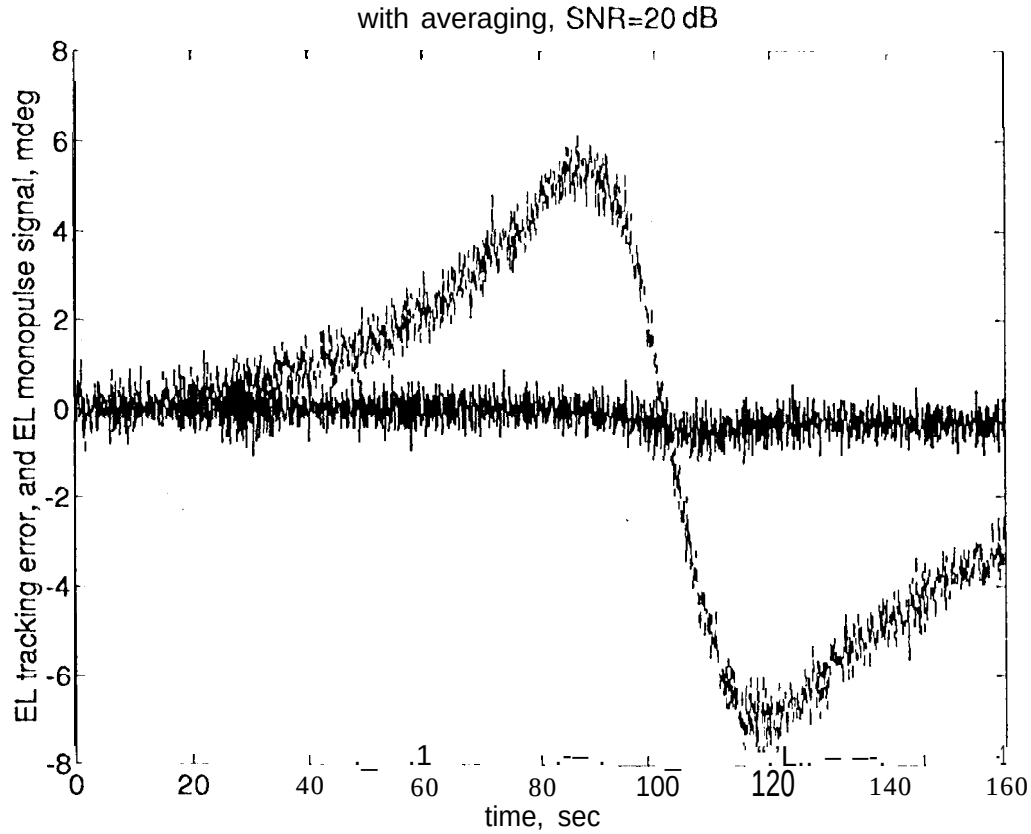

GAWRONSKI, FIG.21